Transport properties of Ce-doped $R\mathrm{MnO_3}$ (R=La, Pr, and Nd) manganites

P. Mandal and S. Das
Saha Institute of Nuclear Physics, 1/AF Bidhannagar, Calcutta 700 064, India
(Received 10 July 1997; revised manuscript received 20 August 1997)

In Ce-doped $R\mathrm{MnO_3}$ the rare earth (R) is partially replaced with cerium ions instead of divalent alkaline-earth metals. These compounds are very sensitive to annealing. The resistivity and thermoelectric power (TEP, S) of $R_{0.7}\mathrm{Ce}_{0.3}\mathrm{MnO_3}$ (R=La, Pr, and Nd) have been studied as a function of annealing conditions. They show a ferromagnetic to paramagnetic transition, and a resistive peak near T_c, marking a metal-insulator (MI) transition. A pronounced giant magnetoresistance effect is also observed in these compounds, and T_c can be changed by annealing in various atmospheres. The $\rho(T)$ curve of oxygen overdoped samples shows double peaks along with a hysteresis loop (in the heating and cooling cycles), which bears the signature of the first-order nature of the transition. The thermopower of as-prepared samples show a peak near the MI transition, and changes sign from positive to negative at temperatures below the ferromagnetic transition. The magnitude of S at low temperatures is enhanced to an abnormally large value. With increasing of oxygen content, several characteristic features develop in the temperature dependence of the thermopower which is consistent with the resistive behavior. At high temperatures, the resistivity and thermopower follow the predictions of the Emin-Holstein theory of adiabatic polaron hopping. [S0163-1829(97)01847-X]

I. INTRODUCTION

The panorama of properties[1–12] exhibited by $R_{1-x}A_x\mathrm{MnO_3}$ (R is a rare earth element and A a divalent alkaline-earth metal), such as giant magnetoresistance (GMR), metal-insulator transition, charge, magnetic ordering, etc., has generated an impulse in the research of rare-earth transition-metal oxide systems, particularly on the interplay among the structure, magnetism, and electronic transport. Depending on the doping level (x) and temperature, these systems present different phases of conduction and complicated magnetic phase transitions. According to the Zaanen-Swatzky-Allen[13] scheme, the parent compound $R\mathrm{MnO_3}$ is a charge-transfer insulator with trivalent manganese in different layers coupled among themselves antiferromagnetically through a superexchange mechanism. But within a layer these Mn^{3+} ions are coupled ferromagnetically. The electronic configuration of Mn^{3+} is $t_{2g}^3 e_g^1$, with a total spin $S=2$. Due to their narrow bandwidth, the tightly bound t_{2g}^3 electrons may be considered as a single localized spin with $S=\frac{3}{2}$. The electrons in the e_g orbital have a strong hybridization with the $2p$ state of a neighboring oxygen ion, and can be localized or itinerant depending on the local spin orientation[14] and carrier density. Holes can be introduced in the manganites by partial substitution of trivalent rare-earth ions with divalent alkaline-earth metals. As a result, the e_g electrons hop between spin-aligned Mn^{3+} and Mn^{4+} ions through oxygen ions. This double-exchange mechanism[15–17] gives rise to metallic conductivity and ferromagnetism in these compounds. However, Ref. 18, the double-exchange mechanism alone cannot explain all the aspects of the GMR effect. The finer details of the resistivity versus temperature curve apparently involves other effects such as charge ordering, size of the cation pairs (R and A) and the polaron effect due to the strong electron-phonon interaction arising from the Jahn-Teller distortion of the Mn^{3+} ions. Due to the vast technological possibility of GMR devices, and the inquisitiveness as to the origin of the mechanism of this effect, a great deal of effort is being devoted in search for materials exhibiting this important property. In generic manganite systems, manganese can have three valence states: Mn^{4+}, Mn^{3+}, and Mn^{2+}. Figure 1 depicts the crystal-field splitting of Mn^{2+}, Mn^{3+}, and Mn^{4+} ions in orthorhombically distorted octahedra. As mentioned above, in a divalent ion-doped manganite system the manganese ion exists in trivalent and tetravalent states, but if the rare-earth ion is partially replaced by some tetravalent ion the corresponding amount of manganese will be converted into a divalent state. Now the question arises whether the double-exchange mechanism and the GMR effect will be inhibited if a tetravalent ion is doped. To investigate in this regard, we studied[19,20] a series of compounds where, instead of a divalent metal ion, we have a doped cerium ion in the $R\mathrm{MnO_3}$ system (R=La, Pr, and Nd). If cerium exists in the tetravalent state as in $\mathrm{CeO_2}$ and $\mathrm{Nd}_{1-x}\mathrm{Ce}_x\mathrm{CuO_4}$, the mixed-valent state of manganese ions will be $\mathrm{Mn}^{3+}/\mathrm{Mn}^{2+}$ instead of $\mathrm{Mn}^{3+}/\mathrm{Mn}^{4+}$. These

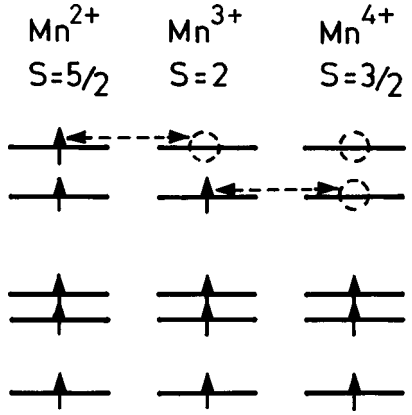

FIG. 1. Crystallographic splitting of Mn^{2+}, Mn^{3+}, and Mn^{4+}, respectively, in orthorhombically distorted octahedra.

compounds show the GMR effect, and a ferromagnetic to paramagnetic transition with an increase of temperature. The ferromagnetism and metallic conductivity appear to be due to the double-exchange interaction between the mixed-valent manganese ions, and their relative amount can be controlled by altering the doping level and oxygen stoichiometry. Since the cerium-doped manganite systems are very sensitive to annealing treatment, annealing at different temperatures and atmospheres can change the oxygen content in the material, thereby influencing their magnetic and electronic properties. Studies of the variation of the electrical conductivity and thermopower with annealing treatment may add valuable information regarding the characteristics of these materials and the electronic nature of the charge carriers in these materials. There are only some scattered reports[21–27] of thermoelectric power (TEP) data of divalent ion-doped manganites. Since in the case of divalent doped manganites the highest T_c and optimum value of GMR have been observed for $x=0.3$, in this paper we confined our studies on $R_{0.7}Ce_{0.3}MnO_3$ systems, and carried out electrical resistivity and thermopower measurements as a function of temperature for samples treated at different annealing conditions.

II. SAMPLE PREPARATION AND EXPERIMENTAL TECHNIQUES

Samples of nominal composition $R_{0.7}Ce_{0.3}MnO_3$ (R=La, Pr, and Nd) were prepared by conventional solid-state reaction methods. A stoichiometric mixture of La_2O_3 (or Pr_6O_{11}/Nd_2O_3), CeO_2, Mn_2O_3 powders was heated in air at 1100 °C for 48 h with intermediate grindings. The La_2O_3 powder was preheated at 900 °C for 12 h. The reacted powder was ground, pelletized, and sintered at 1100 °C for 96 h with two intermediate grindings for homogenization. For Pr- and Nd-based samples, a final sintering process was carried out at 1400 °C for 24 h, and the samples were furnace cooled to room temperature. The as-prepared $La_{0.7}Ce_{0.3}MnO_3$ (sample A) was annealed at 1050 °C in oxygen (sample B), at 900 °C in oxygen at 3-atm pressure (sample C) and at 1400°C in air (sample D) for 24 h to vary the oxygen content. Another sample (sample E) was annealed in oxygen at 900 °C and 3-atmospheric pressure similar to sample C, but for a longer duration. The phase purity was checked by powder x-ray diffraction using Cu $K\alpha$ radiation. The electrical resistance was measured employing the standard four-probe technique in a closed-cycle refrigerator, and a helium cryostat in the temperature range of 4.2–300 K. The thermopower was measured from 77 to 315 K by an automated standard dc method using a differential technique, where a temperature gradient was created across the sample and the voltage δE developed between the hot and cold ends of the thermocouple formed by the sample and Cu wires was measured. The temperature of the sample and temperature difference across the sample were measured using chromel-alumel thermocouples. The samples were attached by pressure contact between two copper blocks, and the whole system was placed in a glass dewar. The TEP was calculated from the slope of the δE versus δT curve.

III. EXPERIMENTAL RESULTS AND DISCUSSION

A. Structural analysis

The room-temperature x-ray-diffraction patterns for $La_{0.7}Ce_{0.3}MnO_3$, $Pr_{0.7}Ce_{0.3}MnO_3$, and $Nd_{0.7}Ce_{0.3}MnO_3$ are shown in Fig. 2. The x-ray-diffraction patterns show that all the samples are single phase. The lattice parameters are determined by least-square fitting of the diffraction profiles in the range $20°\leqslant 2\theta \leqslant 80°$. For both $La_{0.7}Ce_{0.3}MnO_3$ and $Pr_{0.7}Ce_{0.3}MnO_3$, indexes could be assigned to all the lines on the basis of an orthorhombic symmetry. However, the orthorhombic distortion for the latter system is very small. The analysis of the diffraction pattern of the $Nd_{0.7}Ce_{0.3}MnO_3$ sample reveals that the crystallographic unit cell is tetragonally distorted. The room-temperature lattice constants of these samples are presented in Table I. The x-ray-diffraction pictures of $La_{0.7}Ce_{0.3}MnO_3$ samples show only a change in the degree of orthorhombocity with oxygen content, but no secondary phase. Table I shows that the oxygen-deficient as-prepared $La_{0.7}Ce_{0.3}MnO_3$ sample has lattice parameters which are larger than those of oxygen-rich $La_{0.7}Ce_{0.3}MnO_3$ samples.

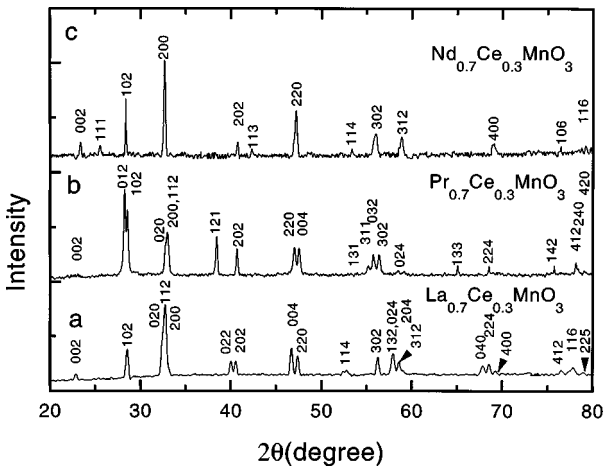

FIG. 2. X-ray powder diffraction patterns of (a) $La_{0.7}Ce_{0.3}MnO_3$ (sample A), (b) $Pr_{0.7}Ce_{0.3}MnO_3$, and (c) $Nd_{0.7}Ce_{0.3}MnO_3$ at room temperature.

B. Resistivity

Figure 3 presents the temperature dependence of the zero-field resistivity of $La_{0.7}Ce_{0.3}MnO_3$ samples annealed at different atmosphere. The $\rho(T)$ curve of sample A exhibits a peak at a temperature T_R. The temperature coefficient $d\rho/dT$ changes its sign at T_R, showing a metal ($d\rho/dT > 0$) to insulator ($d\rho/dT < 0$) transition. With the increase of oxygen content, the conductivity increases, and the resistivity peak becomes sharper and shifts toward higher temperature. Sample D (annealed at 1400 °C in air) shows no resistive peak over the whole temperature range studied, and behaves like an insulator. A marked peculiarity develops in the

TABLE I. Room-temperature crystallographic lattice parameters.

Sample	Symmetry	a(A°)	b(A°)	c(A°)	V(A°^{3})
$La_{0.7}Ce_{0.3}MnO_3$ (A)	orthorhombic	5.411	5.525	7.756	231.87
$La_{0.7}Ce_{0.3}MnO_3$ (C)	orthorhombic	5.403	5.518	7.759	231.32
$Pr_{0.7}Ce_{0.3}MnO_3$	orthorhombic	5.407	5.482	7.667	227.29
$Nd_{0.7}Ce_{0.3}MnO_3$	tetragonal	5.431	5.431	7.675	226.38

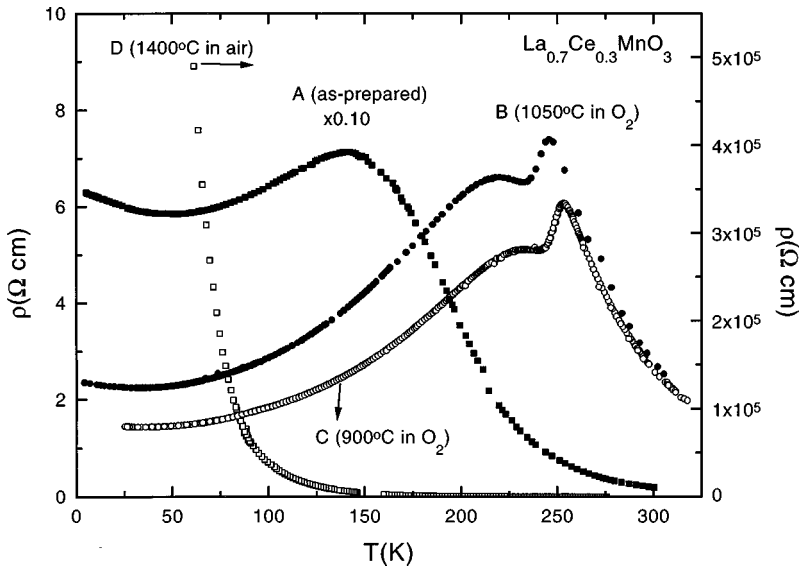

FIG. 3. Temperature dependence of the resistivity of $La_{0.7}Ce_{0.3}MnO_3$ annealed at different atmosphere. Sample A: as-prepared. Sample B: annealed at 1050 °C in air. Sample C: Annealed at 900 °C in 3-atm pressure of oxygen. Sample D: annealed at 1400 °C in air.

temperature-dependent characteristics of the resistivity with the increase of oxygen concentration. The $\rho(T)$ curves show a broad peak at lower temperature (T_{R1}), and a sharp and larger peak at higher temperature (T_{R2}). Initially, a weak shoulderlike feature at lower temperature and a sharp peak at higher temperature have been observed. This shoulderlike feature grows into a peak, and its height increases with oxygen overdoping. The shoulderlike feature has also been observed for oxygenated $La_{2/3}Ba_{1/3}MnO_3$ samples.[28] Figure 4 shows the resistivity versus temperature curve of sample E annealed similarly as sample C, but for a longer duration. This curve also contains a broad and sharp peaklike sample C, but, due to the higher oxygen content the conductivity of this sample increases, and the resistivity peaks shift to higher temperatures. Moreover, the two peaks attain the same height, with the resistivity amplitude of the sharp peak decreased. The resistivity of this sample is strongly dependent on its thermal history, and a trace of the resistivity as a function of temperature in the cooling and heating cycles form a small hysteresis loop around the peak region. This indicates the first-order nature of this transition in the vicinity of the double peaks caused by the oxygen overdoping. Such thermal hysteresis was also observed in $La_{0.825}Sr_{0.175}Mn_{0.94}Mg_{0.06}O_3$ sample,[29] and in Ca-doped $LaMnO_3$ (Ref. 30) and $PrMnO_3$ (Ref. 31) samples. At low temperatures the resistivity does not fall with decreasing temperature, especially in case of samples A and B. Instead there is a slight upturn in $\rho(T)$ at low temperatures, indicating the possible appearance of some kind of localization in these samples in the low-temperature region. The resistivity of the samples increases with the increase of the oxygen deficiency, with a gradual shift of the resistive peak toward lower temperature, and the sample finally reaches an insulating state (sample D). It has been suggested that the increase of oxygen content due to different annealing atmosphere enhances the inherent nonstoichiometry of the manganite system, and the excess oxygen was found not to occupy interstitial positions but to produce vacancies both at the rare-earth and transition-metal sites.[32–35] Moreover, oxygen annealing changes the ratio of the amount of two heterovalent Mn ions, and hence affects the double exchange and conduction process. The variation of the resistivity behavior

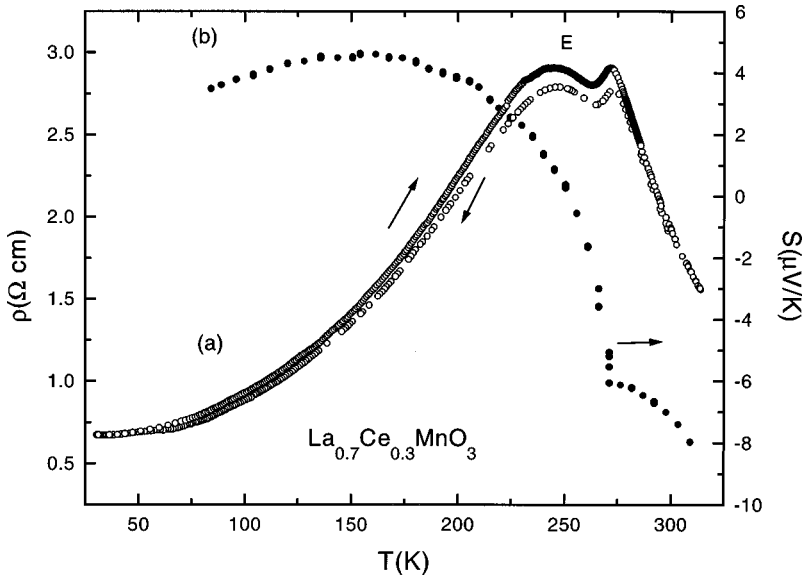

FIG. 4. (a) Resistivity vs temperature for sample E. Sample E is annealed in the same condition as sample C, but for a longer duration. (b) Temperature variation of absolute thermopower of sample E .

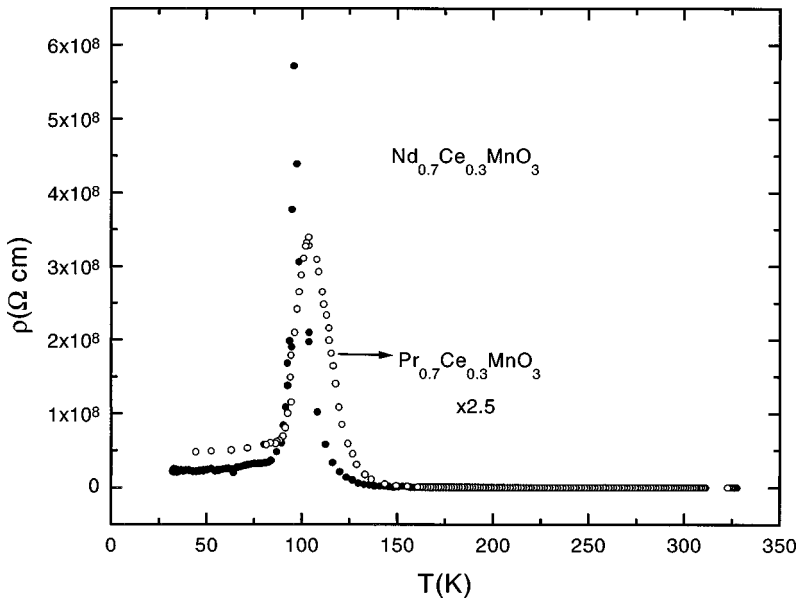

FIG. 5. Temperature dependence of resistivity of (a) $Pr_{0.7}Ce_{0.3}MnO_3$ and (b) $Nd_{0.7}Ce_{0.3}MnO_3$.

of Ce-doped $R\mathrm{MnO}_3$ with annealing environments has a similarity to that of divalent ion-doped $R\mathrm{MnO}_3$ (Refs. 28, 36, and 37). This study shows that the oxygen content regulates the resistivity behavior of these compounds.

The samples show a ferromagnetic to paramagnetic transition[19,20] with an increase of temperature, and usually the magnetic transition occurs at a temperature T_c slightly lower than T_{R1} and T_{R2}. The magnetization of sample A changes from a ferromagnetic to a paramagnetic state at a very slow rate, while sample B shows a very sharp transition. The application of the magnetic field suppresses the resistive peaks drastically, and produces a giant magnetoresistance effect. For samples A and B the magnetoresistance ratio $[\rho(0)\text{-}\rho(H)]/\rho(0)$ reaches about 54% and 46%, respectively, at a 7.7-T field.[19,20] In the case of sample B the magnetic field does not change the nature and position of the broad peak very much, but suppresses the second one greatly, shifting it towards higher temperatures, and the $\rho(T)$ curve bears a resemblance to the peak, with only a shoulderlike feature. The magnetoresistance also shows a sharp peak very close to the second peak. The difference in the response of the two peaks indicates that they may have different origins.

The magnetotransport properties of polycrystalline samples are very complicated in nature.[28,38,39] Several factors influence both the temperature and magnetic-field dependence of resistivity. Grain boundaries play an important role in the charge scattering process in the polycrystalline manganite samples. Hwang *et al.*[38] studied magnetoresistance on single crystal and polycrystalline $La_{2/3}Sr_{1/3}MnO_3$ samples. The $\rho(T)$ curve of the polycrystalline sample shows a peak at high temperature, and a humplike swelling at lower temperature below this peak. However, this small swelling does not appear in the case of the single crystal. They also observed a marked difference between the field dependence of the resistivity of polycrystalline and single-crystal samples. The magnetoresistance of polycrystalline samples is dominated by the scattering of charge carriers from the grain boundaries, while for single crystals the major contribution comes from the spin fluctuations. The large MR near the second peak (T_{R2}) in the $La_{0.7}Ce_{0.3}MnO_3$ system may also originate from domains. Studies on single crystals and thin films may throw some light on this point.

Figures 5(a) and 5(b) present the temperature variation of ρ of $Pr_{0.7}Ce_{0.3}MnO_3$ and $Nd_{0.7}Ce_{0.3}MnO_3$ samples, respectively, showing similar behavior to that for $La_{0.7}Ce_{0.3}MnO_3$, with a sharp metal-insulator transition near T_c. The Pr-based sample shows a MR ratio of 82.5% at 7.7 T (Ref. 20). The Nd-sample shows a high resistivity at room temperature, and the amplitude of the resistive peak is higher than that for the Pr sample.

In the manganite system at high temperatures the lattice becomes distorted around the electrons in the conduction band, and due to the strong electron-phonon interaction small polarons are formed. Above T_c the thermally activated hopping of these polarons plays an important role. In the adiabatic approximation the authors of Refs. 40–42 proposed a small polaron hopping theory according to which the activated conduction follows the relation $\rho(T) = BT\exp(E_\rho/k_BT)$, where k_B is the Boltzmann constant, B the resistivity coefficient, and E_ρ is the activation energy. We plot the high-temperature resistivity as $\log_{10}(\rho/T)$ vs $1000/T$ in Fig. 6(a), and as $\log_{10}(\rho)$ vs $1000/T$ in Fig. 6(b). For the same temperature range the data fit nicely with a straight line for both cases. Thus, from the analysis of the temperature dependence of the resistivity, it is very difficult to distinguish between adiabatic small polaron hopping and activation-type conduction. The activation energies are calculated as 181, 212, and 210 meV from the slope of the linear part of the curves in Fig. 6(a), and 165, 201, and 197 meV from those of the curves in Fig. 6(b) for La, Pr, and Nd samples, respectively. Worledge *et al.*[42] measured the resistivity of a series of argon-annealed $La_{2/3}Ca_{1/3}MnO_3$ films, and analyzed the high-temperature data using different models such as activated conduction, variable range hopping, adibatic and nonadiabatic small polaron hopping. They observed that the adiabatic small polaron hopping model fits better than other models. Perhaps the conduction in the high-temperature region also is governed by the adiabatic small polaron hopping

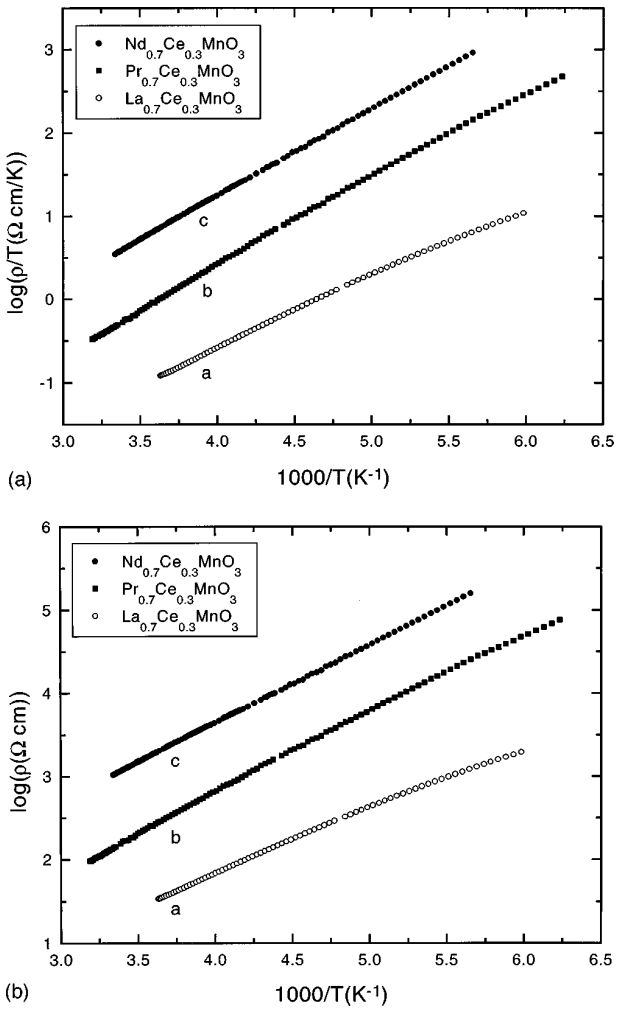

FIG. 6. (a) $\mathrm{Log}_{10}(\rho/T)$ vs $1000/T$ plot for (a) $La_{0.7}Ce_{0.3}MnO_3$ (sample D), (b) $Pr_{0.7}Ce_{0.3}MnO_3$, and (c) $Nd_{0.7}Ce_{0.3}MnO_3$. (b) $\mathrm{Log}_{10}(\rho)$ vs 1000/T plot for (a) $La_{0.7}Ce_{0.3}MnO_3$ (sample D), (b) $Pr_{0.7}Ce_{0.3}MnO_3$, and (c) $Nd_{0.7}Ce_{0.3}MnO_3$.

mechanism in the Ce-doped manganites. An analysis of the temperature dependence of the resistivity and thermopower together may help in this regard.

C. Thermopower

The temperature dependences of the thermopower of as-prepared La-, Pr-, and Nd-based manganites are shown in Fig. 7. As the temperature decreases from 300 K the TEP increases slowly, reaches a maximum value at around the metal-insulator (MI) transition point, and then falls sharply with a further decrease of temperature. At low temperatures below T_c, the TEP changes its sign from positive to negative, and finally attains a very high value (2500, 4750, and 24500 μV/K for La, Pr, and Nd samples, respectively). These values are much larger than that of divalent ion doped manganite systems. It should be mentioned here that although there is a noticeable difference in the low-temperature values of S of these samples, the room temperature magnitude of S is small and comparable. At present we do not know the origin of such unusually large values of S at low temperatures. Above T_c the behavior of the TEP is consistent with the characteristic of insulator or semiconductor, i.e., $|S|$ enhances with the decrease of temperature, while, below T_c the nature of the TEP corresponds to the metallic characteristic, i.e., $|S|$ decreases with the fall of temperature. The thermal variation of the TEP bears a close resemblance to that of the resistivity. Figure 8 presents the temperature dependence of the thermopower for $La_{0.7}Ce_{0.3}MnO_3$ samples treated at different annealing conditions. For all the samples the thermopower is positive throughout the temperature range studied. The value of S of these samples is much smaller than that of as-prepared samples. For samples B and C the TEP increases slowly, passes through a broad maximum, falls to a minimum value, and then increases again very slowly until it attains a saturation value ~ 5 μV/K. The S of sample D shows a broadened peak, and, at low temperature, S falls nearly to zero with a tendency of sign change from positive to negative with a further decrease of temperature. It should be mentioned here that the $\rho(T)$ curve of this

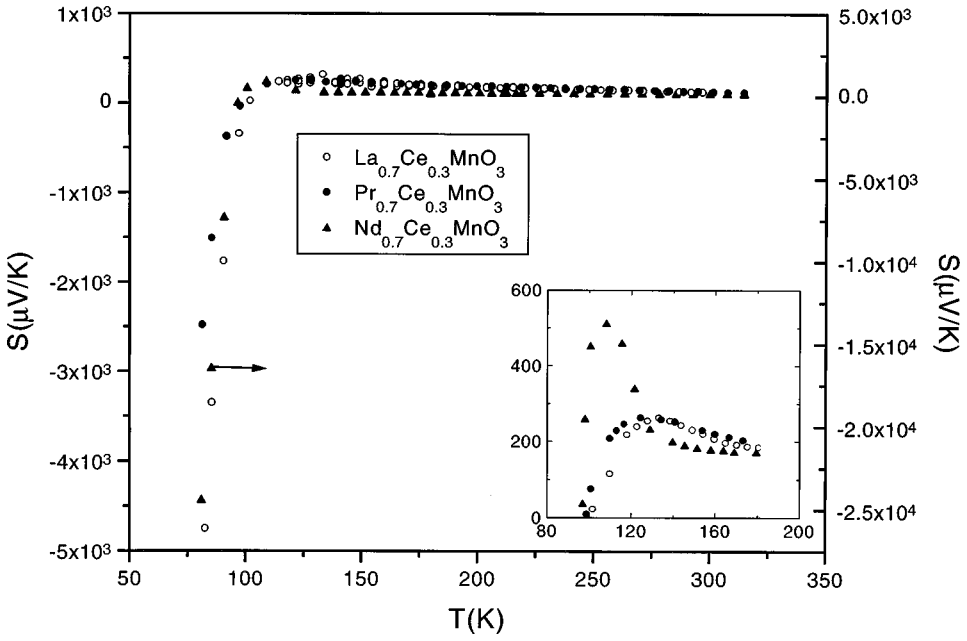

FIG. 7. Temperature dependence of absolute thermopower S for samples (a) $La_{0.7}Ce_{0.3}MnO_3$ (sample A), (b) $Pr_{0.7}Ce_{0.3}MnO_3$, and (c) $Nd_{0.7}Ce_{0.3}MnO_3$. Inset shows the variation of S near the transition point.

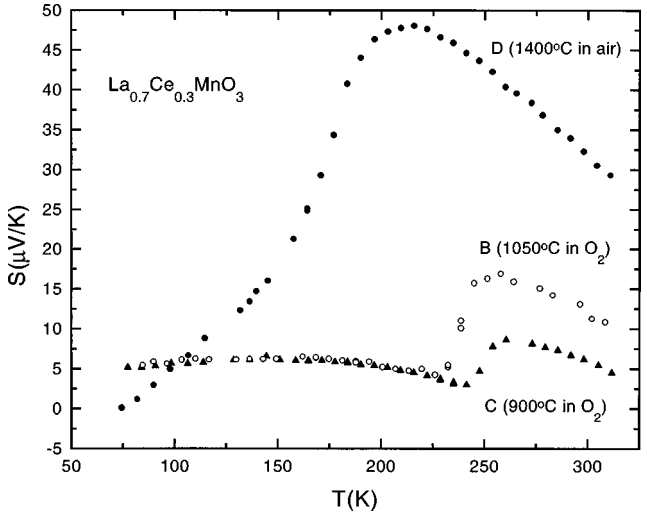

FIG. 8. Influence of annealing conditions on the temperature dependence of thermopower for $La_{0.7}Ce_{0.3}MnO_3$ (samples A, B, C, and D).

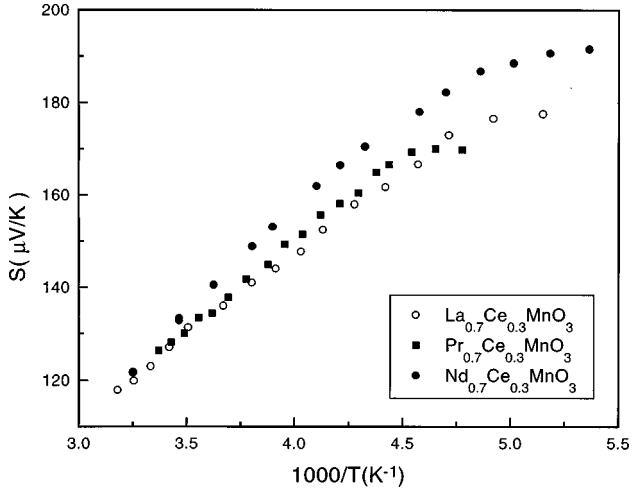

FIG. 9. Thermopower vs the inverse-temperature for (a) $La_{0.7}Ce_{0.3}MnO_3$ (sample D), (b) $Pr_{0.7}Ce_{0.3}MnO_3$, and (c) $Nd_{0.7}Ce_{0.3}MnO_3$.

sample shows no peak. The thermopower of oxygen annealed La sample (E) is negative (~ -8 μV/K) at 300 K (Fig. 4). Initially S increases slowly with a decrease of temperature, and then shows a steplike increase. Thus S shows two characteristic temperatures: a kinklike feature, i.e., dS/dT is discontinuous at 272 K, and the change of sign of S from negative to positive at 250 K. These two characteristic temperatures correspond to the temperatures of the sharper and broader resistive peaks. If the sign of the TEP upholds the nature of the charge carriers, then all along the positive value of S indicates the holelike character of the carriers. The sharp increase of S near T_c reflects the sudden change of spin entropy due to the enhancement of the spin polarization caused by magnetic transition.

If the spin-dependent contribution is neglected, then Mott's formula[43] for the charge contribution to the TEP can explain the metallic conduction of the $S(T)$ curve in the low temperature region and can be expressed as $S=(\pi^2 k_B{}^2 T/3e)[dln\sigma(E)/dE]_{E=E_F}$, where $d\sigma(E)/dE$ is the energy derivative of the conductivity $\sigma(E)$, and E_F is the Fermi energy in the vicinity of which charge carriers dominate the transport process. This expression can explain the small value and weak temperature dependence of S in the low-temperature ferromagnetic state (Figs. 4 and 8). A weak energy dependence of conductivity $\sigma(E)$ is implied in the observed small value of the TEP at low temperature. Pickett and Singh[44] used self-consistent local spin-density-functional methods to study the electronic structure of $La_{1-x}Ca_xMnO_3$, and the effect of hybridization on it. The majority channel consists of two strongly overlapping e_g-derived $dp\sigma$ bands crossing the Fermi level (E_F), whereas for the minority channel there is a gap between O $2p$ bands and Mn $3d$ bands which extends up to E_F. It was found that strongly hybridized bands produce a partially open shell oxygen ion in the majority-spin channel and this may well explain the metallic conduction at low temperature. Pickett and Singh considered the local environment effects of Mn due to the relative number of Ca^{2+} and La^{3+} cations surrounding the Mn ions. Considering the doping as an ordered supercell of 2+ and 3+ ions, they found that the bands obtained from Mn atoms neighboring 3+ atoms have lower energy than the bands from Mn atoms close to 2+ ions. Such a superlattice generates ladder- or step-function-like energy-band offsets. The cation disorder distorts the super cell structure, and the scattering potential thus produced broadens the energy band in effect. Due to the energy dependence of interband scattering in the band offsets, the conductivity varies nonmonotonically with energy. The thermal broadening of the Fermi surface causes a sign reversal of the thermopower. Near the magnetic transition the Mn-derived majority and spin minority bands collapse into a band of disorder-broadened and partially occupied electronic states. The temperature dependence of the electronic structure causes the temperature dependence of the TEP below the transition. Crespi *et al.*[21] used these arguments to explain the TEP data of their Nd-based samples below the temperature corresponding to the resistive peak. They proposed that the temperature dependence of the thermopower above T_c should also reflect the hopping of polarons. In our samples Mn has two distinct sites: one ($Mn_{R\text{-}R}$) sandwiched between R^{3+}-R^{3+} layers, and the other ($Mn_{R\text{-}Ce}$) between layers of R^{3+}-Ce ion. We think a similar explanation will also be valid in our case for TEP below the resistive transition temperature. According to the adiabatic small polaron hopping theory the thermopower can be expressed as $S(T)=(k_B/e)[\alpha + E_S/k_BT]$, where E_S is the activation energy for the TEP, and α is the sample-dependent constant. In the high-temperature regime above the resistive transition, the thermopower for the samples studied here obeys the prediction of the adiabatic small polaron hopping theory, since S vs $1000/T$ curves fit well with straight lines (Fig. 9). From the linear fit of the curves we obtain the activation energies for thermopower as $E_S=35.6$, 40.3, and 43.5 meV for La, Pr, and Nd samples, respectively. Since the resistivity and thermopower show different values for the activation energy, we may conclude that charge transport occurs due to the hopping of carriers rather than semiconductinglike activated conduction.

IV. CONCLUSIONS

In conclusion, we can summarize the results as follows. The $\rho(T)$ curves have the following special features: (1) The

high-temperature semiconducting or insulating region is characterized by conduction obeying the Emin-Holstein theory of adiabatic polaron hopping. (2) There is a paramagnetic insulator to ferromagnetic metal transition in the intermediate temperature region, and the MI transition is very sharp for Pr- and Nd-based samples with very large resistive values. (3) The low-temperature region is marked by relatively large values of the residual resistivity (especially for as-prepared samples). (4) Double peaks appear in the $\rho(T)$ curve of $La_{0.7}Ce_{0.3}MnO_3$, and shift toward higher temperature, and the amplitude decreases with the increase of the oxygen content. (5) A thermal hysteresis occurs in the $\rho(T)$ curve in the heating and cooling cycles. The thermal behavior of thermopower can be divided into three regions: (1) a low-temperature region with a drop of the thermopower from large to small values, characteristic of metals for oxygenated samples, and a sharp drop from positive to unusually large negative value for as-prepared samples; (2) an intermediate-temperature region of the TEP, showing a peak near T_c and a change of sign below T_c; and (3) a high-temperature region with polaronic hopping behavior. The observed large difference between the activation energies (obtained from the analysis of the temperature dependence of the resistivity and thermopower in the temperature region above T_c) upholds the polaronic nature of the charge carriers above T_c. In the double-exchange model the Mn ions should exist in the mixed-valence state for the GMR effect to appear and to maintain the correlation between the magnetism and conductivity in the manganite system. In the divalent ion-doped manganites, Mn ions appear in the trivalent and tetravalent states in a proportion depending upon the doping content. In order to understand the doping process and the physical properties of the Ce-doped manganites properly, a determination of the valence states of Ce and Mn ions is very essential. In oxides of Ce, Ce exhibits a mixed-valent character with a valency between 3 and 4. The core-level photoemission and x-ray-absorption measurements[45] of CeO_2 and $Nd_{2-x}Ce_xCuO_4$ show that Ce has an intermediate valence state of $3.5+$, arising from the hybridization with the O $2p$ band. If such a doping mechanism becomes operative in the Ce-doped manganite, then the Mn valence is expected to be Mn^{3+}/Mn^{2+}, which makes a sharp contrast with the case in the divalent ion-doped ones. Therefore, it is felt that the determination of the valency of the doped Ce ion and the consequent change of the valence state of Mn ions are very much essential to understand the origin of magnetotransport properties in this system.

ACKNOWLEDGMENT

We are grateful to Professor B. Ghosh for helpful discussions and encouragement.

[1] G. H. Jonker and J. H. Van Santen, Physica (Amsterdam) **16**, 337 (1950); **16**, 599 (1950).
[2] G. H. Jonker, Physica (Amsterdam) **22**, 707 (1956).
[3] R. von Helmholt, J. Wecker, B. Holzapfel, M. Shultz, and K. Samwer, Phys. Rev. Lett. **71**, 2331 (1993).
[4] R. M. Kusters, J. Singleton, D. A. Keon, R. M. Greedy, and W. Hayes, Physica B **155**, 362 (1989).
[5] K. Chahara, T. Ohno, M. Kasai, and Y. Kozono, Appl. Phys. Lett. **63**, 1990 (1993).
[6] S. Jin, T. H. Tiefel, M. McCormack, R. A. Fastnacht, R. Ramesh, and L. H. Chen, Science **264**, 413 (1994).
[7] Y. Tomioka, A. Asamitsu, Y. Moritomo, H. Kuwahara, and Y. Tokura, Phys. Rev. Lett. **74**, 5108 (1995).
[8] H. Kuwarhara, Y. Tomioka, A. Asamitsu, Y. Moritomo, and Y. Tokura, Science **270**, 961 (1995).
[9] P. Schiffer, A. P. Ramirez, W. Bao, and S.-W. Cheong, Phys. Rev. Lett. **75**, 3336 (1995).
[10] J. M. D. Coey, M. Viret, L. Ranno, and K. Ounadjela, Phys. Rev. Lett. **75**, 3910 (1995).
[11] P. G. Radaelli, D. E. Cox, M. Marezio, and S.-W. Cheong, Phys. Rev. B **55**, 3015 (1997).
[12] A. Asamitsu, Y. Moritomo, Y. Tomioka, T. Arima, and Y. Tokura, Nature (London) **373**, 407 (1995).
[13] J. Zaanen, G. A. Sawatzky, and J. W. Allen, Phys. Rev. Lett. **55**, 418 (1985).
[14] J. B. Goodenough, Prog. Solid State Chem. **5**, 145 (1971).
[15] C. Zener, Phys. Rev. **82**, 403 (1951).
[16] P. W. Anderson and H. Hasegawa, Phys. Rev. **100**, 675 (1955).
[17] P. G. de Gennes, Phys. Rev. **118**, 141 (1960).
[18] A. J. Millis, P. B. Littlewood, and B. I. Shraiman, Phys. Rev. Lett. **74**, 5144 (1995).
[19] S. Das and P. Mandal, Indian J. Phys. **71**, 231 (1997).
[20] S. Das and P. Mandal, Z. Phys. B **104**, 7 (1997).
[21] V. H. Crespi, Li Lu, X. Jia, K. Khazeni, A. Zettl, and M. L. Cohen, Phys. Rev. B **53**, 14 303 (1996).
[22] M. Jaime, M. B. Salamon, M. Rubinstein, R. E. Treece, J. S. Horwitz, and D. B. Chrisey, Phys. Rev. B **54**, 11 914 (1996).
[23] A. Asamitsu, Y. Moritomo, and Y. Tokura, Phys. Rev. B **53**, 2952 (1996).
[24] B. Fisher, L. Patlagan, and G. M. Reisner, Phys. Rev. B **54**, 9359 (1996).
[25] J. Hejtmanek, Z. Jirak, D. Sedmidubsky, A. Maignan, Ch. Simon, V. Caignaert, C. Martin, and B. Raveau, Phys. Rev. B **54**, 11 947 (1996).
[26] B. Fisher, L. Patlagan, G. M. Reisner, and A. Knizhnik, Phys. Rev. B **55**, 9227 (1997).
[27] M. F. Hundley and J. J. Neumeier, Phys. Rev. B **55**, 11 511 (1997).
[28] H. L. Ju, J. Gopalakrishnan, J. L. Peng, Qi Li, G. C. Xiong, T. Venkatesan, and R. L. Greene, Phys. Rev. B **51**, 6143 (1995); M. Dominguez *et al.*, Europhys. Lett. **32**, 349 (1995).
[29] A. Anane, C. Dupas, K. Le Dang, J.-P. Renard, P. Veillet, A. M. de Leon Guevara, F. Millot, L. Pinsad, A. Revcolevschi, and A. G. M. Jansen, J. Magn. Magn. Mater. **165**, 377 (1997).
[30] H. Y. Hwang, S.-W. Cheong, P. G. Radaelli, M. Marezio, and B. Batlogg, Phys. Rev. Lett. **75**, 914 (1995).
[31] Y. Tokura, A. Urushibara, Y. Moritomo, T. Arima, A. Asamitsu, G. Kido, and N. J. Furukawa, J. Phys. Soc. Jpn. **63**, 3931 (1994).
[32] J. A. M. van Roosmalen, E. H. P. Cordfunke, R. B. Helmholdt, and H. W. Zandbergen, J. Solid State Chem. **110**, 100 (1994).
[33] J. A. M. van Roosmalen and E. H. P. Cordfunke, J. Solid State Chem. **110**, 106 (1994).

[34] J. A. M. van Roosemalen and E. H. P. Cordfunke, J. Solid State Chem. **110**, 109 (1994).
[35] J. A. M. van Roosemalen, P. van Vlaanderen, and E. H. P. Cordfunke, J. Solid State Chem. **114**, 516 (1990).
[36] J. Pierre, F. Robaut, S. Misat, P. Strobel, A. Nossov, V. Ustinov, and V. Vassiliev, Physica B **225**, 214 (1996).
[37] A. Nossov, J. Pierre, V. Vassiliev, and V. Ustinov, Solid State Commun. **101**, 361 (1997).
[38] H. Y. Hwang, S-W. Cheong, N. P. Ong, and B. Batlogg, Phys. Rev. Lett. **77**, 2041 (1996).
[39] A. Gupta, G. Q. Gong, G. Xiao, P. R. Duncombe, P. Lecoeur, P. Trouilloud, Y. Y. Wang, V. P. Dravid, and J. Z. Sun, Phys. Rev. B **54**, R15 629 (1996).
[40] T. Holstein, Ann. Phys. (N.Y.) **8**, 343 (1959).
[41] D. Emin, in *Electronic Structure Properties of Amorphous Semiconductors*, edited by P. G. Le Comber and N. F. Mott (Academic, New York, 1973).
[42] D. C. Worledge, G. Jeffrey Snyder, M. R. Beasley, T. H. Geballe, R. Hiskes, and S. DiCarolis, J. Appl. Phys. **80**, 5158 (1996).
[43] N. F. Mott and E. A. Davis, *Electron Processes in Non-Crystalline Materials*, 2nd ed. (Clarendon, Oxford, 1979).
[44] W. E. Pickett and D. J. Singh, Europhys. Lett. **32**, 759 (1995); W. E. Pickett, D. J. Singh, and E. Letts, Phys. Rev. B **55**, R8642 (1997).
[45] J. M. Tranquada, S. M. Heald, A. R. Moodenbaugh, G. Liang, and M. Croft, Nature (London) **337**, 720 (1989).